Available online at www.sciencedirect.com

SciVerse ScienceDirect

Ceramics International 39 (2013) 4581–4587

CERAMICS INTERNATIONAL

www.elsevier.com/locate/ceramint

Structure and optical properties of iron oxide films prepared by a modified wet-chemical method

G. Carbajal-Franco[a], M. Eastman[b], C.V. Ramana[a,c,*]

[a]Department of Materials Science and Engineering, University of Texas at El Paso, El Paso, TX 79968, USA
[b]Department of Chemistry, University of Texas at El Paso, El Paso, TX 79968, USA
[c]Department of Mechanical Engineering, University of Texas at El Paso, El Paso, TX 79968, USA

Received 13 September 2012; received in revised form 9 November 2012; accepted 20 November 2012
Available online 27 November 2012

Abstract

Iron oxide (α-Fe_2O_3) films were prepared in isopropyl alcohol with the addition of different concentrations of acetic acid (AcOH). The agglomeration properties of nano-particulated iron oxides and hydroxides precipitated from isopropyl alcohol–water solutions differ from those obtained by precipitation from aqueous solution. Subsequent aging of the precipitated oxides and hydroxides in a weak solution of acetic acid modifies their micro/nanostructure. X-ray diffraction and scanning electron microscopy results demonstrate that use of an isopropyl–water reaction medium produces a material with improved dispersion behavior. The homogeneity of films prepared from the reaction products aged in acetic acid (AcOH) shown to depend on the concentration of acetic acid employed. Increasing concentration of AcOH promotes the coarsening of the nanoparticles and the porosity reduction. Optical spectroscopy analysis indicates that band gap of the materials is ~2.16 eV, which expected for α-Fe_2O_3. The crystal structure, morphology and optical absorption studies confirm that it is an efficient method to produce high quality iron oxide films.

Keywords: Iron oxide; Thin films; Wetting; Morphology

1. Introduction

Iron oxides find a wide range of scientific and technological applications, which include photolytic water dissociation [1–7], chemical gas sensing [8,9], and catalysis [10,11]. Recently, there has been increasing attention toward Fe_2O_3 for utilization in photoelectrochemical cells [10–13]. A band gap of 2.2 eV, high affinity towards water and options for facile synthesis makes Fe-oxide interesting for photo-catalytic applications [12,13]. Many of the recent efforts were directed towards fabrication and optical and photo-catalytic properties of Fe-oxides to improve the efficiency [1–5,11,14–17]. In addition, significant attention has been paid toward improving the photo-catalytic response of Fe-oxide by means of doping [14–19], manipulating the micro/nano-structure and related properties [20–22] and some other chemical approaches [23,24].

The crystal structure and morphological characteristics (such as grain size, shape and distribution) and the composition of the Fe-oxide materials grown in liquid media depend on the nature of solvent i.e., aqueous or non-aqueous [25–31]. Furthermore, if the precipitation of the materials is carried out involving water, the products could be hydroxylated [27]. In the other case, where precipitation occurs in a non-aqueous media, the most common condensation steps in the formation of a metal–oxygen–metal bond are as follows: alkyl halide elimination, ether elimination, ester elimination and aldo-like condensation [29]. The shape could also be controlled by the addition of surfactants during the precipitation. The other approach is to modify the micro/nano-structure of the materials. The objective of the present work is to demonstrate an approach to improve the structural characteristics and properties of iron oxide through relatively simple changes in the synthetic procedures. In this work, precipitation reaction to form α-FeO(OH) (Goethite) was carried out in a mixed media composed of water and

*Correspondence to: University of Texas at El Paso, Department of Mechanical Engineering, 500 West University Avenue, El Paso, TX 79968, USA. Tel.: +1 915 747 8690.
E-mail address: rvchintalapalle@utep.edu (C.V. Ramana).

0272-8842/$ - see front matter © 2012 Elsevier Ltd and Techna Group S.r.l. All rights reserved.
http://dx.doi.org/10.1016/j.ceramint.2012.11.055

isopropyl alcohol (IsOH). Following precipitation, acetic acid was used to modify the nano/micro-structure of the iron oxides/hydroxides produced. Inclusion of IsOH in the solvent for the precipitation reaction improves the dispersion of the final material by reducing the agglomeration of the iron hydroxide nano-particles; and the subsequent addition of acetic acid (AcOH) appears to promote the homogeneity and adherence of the final film. The crystal structure, morphology and optical properties of Fe-oxide films prepared using a mixed media composed of water and isopropyl alcohol (IsOH) are presented and discussed in this paper.

2. Experimental section

The raw materials purchased from Sigma Aldrich were employed in the chemical synthesis of Fe oxides. The $Fe(NO_3)_3 \cdot 9H_2O$ and glacial acetic acid employed were ACS Reagent Grade. Ammonia was supplied as a 33 wt% aqueous solution. The isopropyl alchohol (99.55%) was manufactured by BDH chemicals. Initially 30 ml of a 3.52 M aqueous solution of NH_3 was added to 20 ml of an IsOH solution that was 1 M in $Fe(NO_3)_3 \cdot 9H_2O$. The resulting solution was stirred for 5 min. The precipitate which formed was allowed to age for approximately 30 min and was then separated from the liquid by centrifugation. The resulting precipitate was washed 5 times with 50 ml aliquots of IsOH and then suspended in sufficient alcohol to yield a final volume of 30 ml. Six 5 ml samples were prepared and AcOH was added to concentrations of 0, 0.5, 1.0 2.4, 9.1 and 16.7 vol%. Two different sets of film samples were deposited, the first set was deposited the same day as the precipitates were obtained and the second set was deposited after the precipitates were left to age for 1 week. The films were deposited on acetone cleaned glass and p-Si substrates. All the samples were heated to a final temperature of 773 K (heating rate 23 K/min) for 3 h to transform Goethite to α-Fe_2O_3 (Hematite) and to evaporate residual organic compounds to form the final materials. A control sample was synthesized in an aqueous solution, using no IsOH and AcOH. This material produced in this synthesis was deposited on a p-type Si substrate and followed the same heat treatment.

The grown Fe-oxide films were characterized by performing crystal structure, morphology and optical measurements. X-ray diffraction (XRD) measurements were performed by using a Bruker D8 Advance X-ray diffractometer. XRD patterns were recorded using Cu Kα radiation ($\lambda = 1.54056$ Å) at RT. Surface imaging and cross sectional analysis was performed using a high-performance and ultra-high resolution scanning electron microscope (Hitachi S-4800). The secondary electron imaging was performed on Fe-oxide films grown on Si wafers using carbon paste at the ends to avoid charging problems. The optical properties of Fe-oxide films were evaluated using optical transmission measurements using Cary 5000 UV–vis–NIR double-beam spectrophotometer.

3. Results and discussion

All the films exhibit the α-Fe_2O_3 phase (PDF card 01-072-6226) as evidenced from XRD studies. XRD plots of the "same day" films prepared on glass substrates are shown in Fig. 1. The apparent signal to noise ratio in these plots is inversely related to the concentration of AcOH in the coating solutions. The *SNR* can be related to many variables of system under analysis [32–34]. In the case where the intensities of the signals are known, the *SNR* is defined as the power ratio between the signal and the noise in the system. In our particular case, the *SNR* is calculated by

$$SNR = \frac{P_{signal}}{P_{noise}} = \left(\frac{A_{signal}}{A_{noise}}\right)^2 \quad (1)$$

where P is the root square (RMS) value of the XRD power and A is the RMS value of the amplitude. In this work we noted the inverse relation between the *SNR* and the AcOH volume percent concentration for same day samples (black squares) calculated with the RMS values of the (104) plane peak.

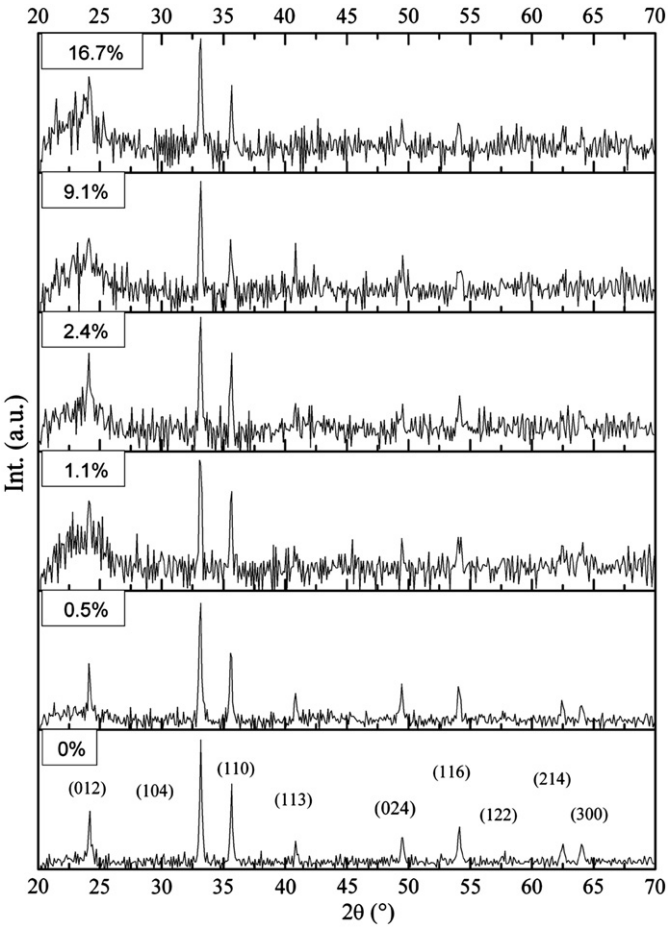

Fig. 1. XRD plots of Fe-oxide films prepared on glass substrates. All the samples were prepared on the same day of preparing sols.

The coherently diffracting domain size (D_{hkl}) was calculated from the integral width of the diffraction lines using the well known Scherrer's equation after background subtraction and correction for instrumental broadening [35,36]. The Scherrer equation is [35,36]

$$D_{hkl} = 0.9\lambda/\beta\cos\theta \quad (2)$$

where D_{hkl} is the size, λ is the wavelength of the filament used in the XRD machine, β is the width of a peak at half of its intensity, and θ is the angle of the peak. By applying Scherrer's formula with the pertinent corrections [35,36],. the average crystallite size measured is 34 nm. It was found that the average crystallite size of the samples is almost constant and uniform; no definite trend is observed with variable AcOH concentration. The wide peak centered $2\theta \approx 22.5^{\circ}$ is due to the effect of the substrate and is also an indication of the reduction of material present in the films. The XRD plot of the samples deposited by spin-coating 1 week after the preparation of the sols is shown in Fig. 2. The apparent signal to noise ratio again decreased for all AcOH concentrations after a full week of aging. The signal to noise ratio also decreases for a specific AcOH concentration when "same day" and "1 week" samples were compared. This can be attributed to a reduction of the amount of material composing the film that can be due to a reduction film thickness and/or cracking upon aging.

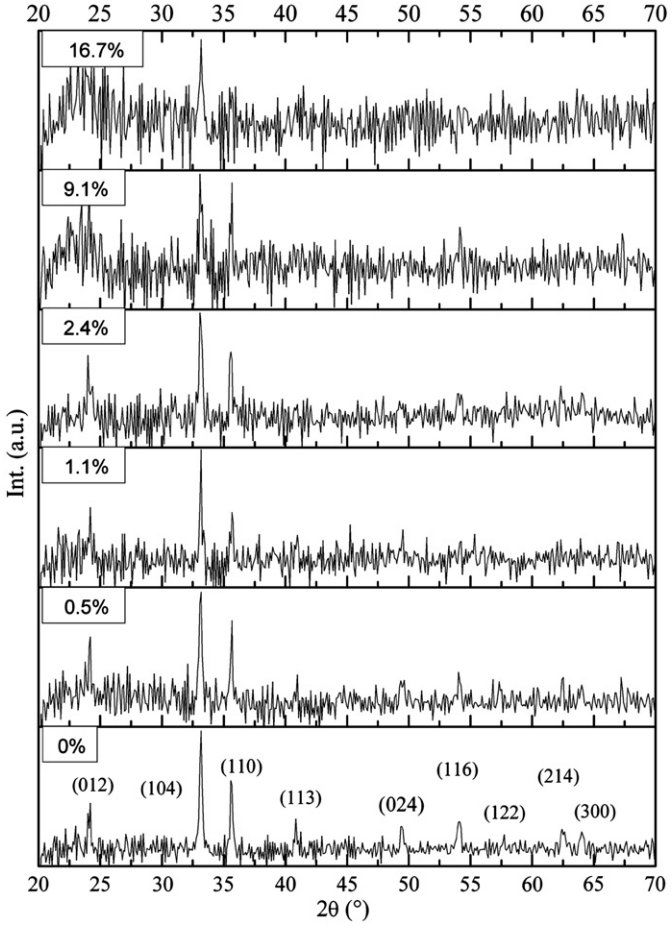

Fig. 2. XRD plot of samples deposited 1 week after preparation of sols.

Fig. 3 shows the SEM images of samples with different conditions of preparation. The image in Fig. 3a was obtained using the control sample, which shows highly agglomerated particles of size ~27 nm (confirmed to be the crystal size by Scherrer's formula, XRD plot not shown). Fig. 3b shows a sample prepared in H_2O–IsOH without any addition of AcOH (0 vol%). The particle size is ~35 nm, same as the crystal size as determined by XRD analysis. This observation indicates that each of the particles is a hematite crystal. The difference in agglomeration between samples prepared in aqueous media and mixed media solvents is clearly evident in these micrographs. In the mixed media-solvent prepared samples, the particles are dispersed in a way that leaves large porous material with sizes comparable with the particle size. Fig. 3c corresponds to a sample prepared in H_2O–IsOH and 1.1 vol% of added AcOH. The difference of this sample with the 0 vol% of AcOH sample is almost negligible in terms of nanostructure, but the effect of the addition of the AcOH is evident as the concentration is increased. Comparing the samples with 2.4, 9.1 and 16.7 vol% of AcOH (Fig. 3d–f) it can be seen that the particles present an evident increase in the coarsening. On the sample prepared with 2.4 vol% (Fig. 3d) the coarsening starts to close the pores that are almost disappear for samples with 9.1 and 16.7 vol% of added AcOH. The effect of mixed media is remarkable in improving the morphological characteristics of Fe-oxide films.

The chemistry involved in improved morphology of Fe-oxide films prepared with mixed media can be understood as follows. The change in the coarsening of the nano-particles can be attributed to the slow rate of reactions occurring on the surface of the nano-particles. As the AcOH was added after the goethite precipitates, it is expected that hydrogen bonding [37] involving the oxygen and hydroxyl groups on the surface of the nano-particles and the AcOH will lead to a partial coverage of the nano-particles surface by AcOH molecules with the extent of coverage dependent on the concentration of AcOH. In addition to the coverage of the surface of the particle with AcOH, it is also possible that iron acetates (FeAc) form which can be the promoters of the coarsening of the nano-particles. The molecules of FeAc can remain hydrogen-bonded to the particles and to the AcOH on the surface. When heated, all the organic compounds evaporate and decompose [38,39] leaving a sample formed only by iron oxide. This effect of the AcOH on the iron hydroxide was previously observed and described by the authors, occurring on materials prepared in aqueous media [31].

The surface imaging analysis of the samples deposited by the spin-coating technique onto silicon substrates is shown in Fig. 4. The effect of AcOH exposure on the distribution of the material on the surface of the silicon substrate is evident. With 0 vol% of AcOH (Fig. 4a) the sample do not

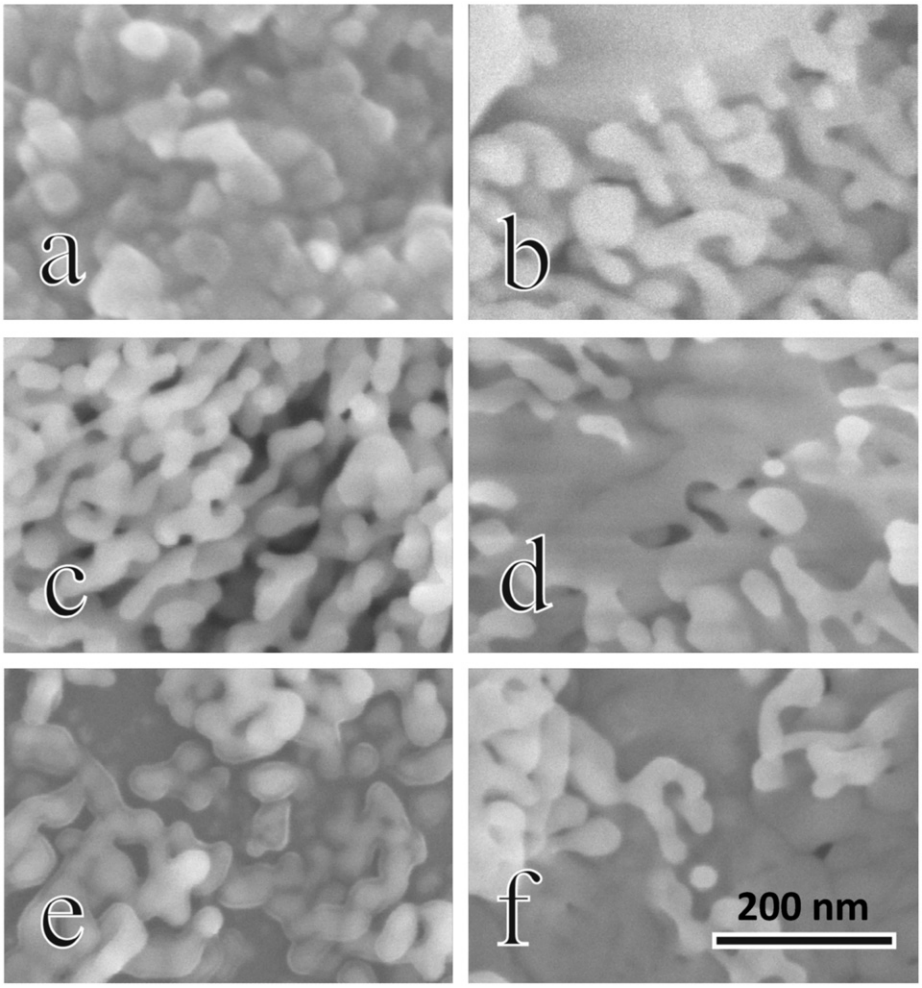

Fig. 3. Samples deposited by the spin-coating method on silicon substrates 1 week after the preparation of the sols. Samples prepared in (a) water and 0 vol% AcOH, (b) IsOH and 0 vol% AcOH, (c) IsOH and 1.1 vol%, (d) IsOH and 2.4 vol%, (e) IsOH and 9.1 vol% and (f) IsOH and 16.7 vol%. Scale bar is 200 nm and applies to all images.

attach adequately to the surface, leaving islands all around the substrate and the material can easily detached from the surface in the form of flakes. The formation of islands is due to the cracking of the film during its drying and the poor bonding of the material to the substrate. The addition of 0.5 vol% of AcOH (Fig. 4b) promotes the homogeneity of the film, leaving an apparent full coverage at the down-left corner of the image (corresponding to the center of the substrate). The cracks on the up-right corner are due to the shrinkage of the material when drying and are prominent because film thickens is larger than at the center of the substrate. Fig. 4c and d presents the samples with 1.1 and 9.1 vol% of added AcOH. The effect of the AcOH is not distinguishable at this magnification. The effect of the cracking is closely related to the film thickness [40]; thicker films tend to show higher cracking in amount and size. Based on these concepts, it is clear that the samples with AcOH tend to be thinner in proportion to the concentration of the added AcOH. This can be verified using XRD results and analysis; it was previously mentioned that higher concentrations of AcOH promotes a decrease in the amount of the material composing the film and it is not due to the loss of material because of poor adhesion of the film to the substrate as seen in Fig. 4a.

In order to be able to have an idea of the quality of the coverage of the film on the substrate, Fig. 5 presents the images of the same samples shown in Fig. 4 but at higher magnification. Fig. 5a shows the areas between the islands; evident is the absence of sample on large regions of the surface. The cracking of the sample in Fig. 5b (0.5 vol% of AcOH) is almost 10 times smaller than the cracking showed in Fig. 5a (0 vol% of AcOH). This is an indication of the effect of the AcOH on the cracking of the film even at a low concentration of 0.5 vol% of AcOH. For samples with higher concentrations of AcOH, the cracking is almost negligible at this magnification.

The optical characteristics of the samples obtained in the present work are shown in Figs. 6 and 7. The plot of the transmittance vs. (photon) energy is shown in Fig. 6. The reduced amounts of material and the non-homogeneity make impossible to use standard methods for band gap calculations (absorption constant, OD plots) [41]. Because

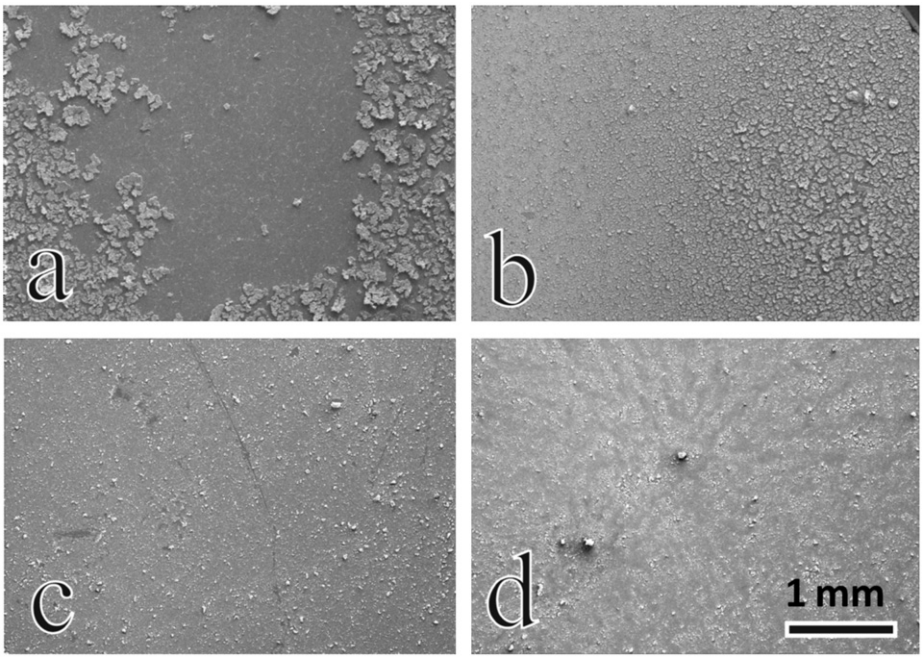

Fig. 4. Samples deposited by the spin-coating method on silicon substrates 1 week after the preparation of the sols. Samples prepared in isopropanol and (a) 0 vol% AcOH, (b) 0.5 vol% AcOH, (c) 1.1 vol% AcOH and (d) 9.1 vol% AcOH. Scale bar is 1 mm and applies to all images.

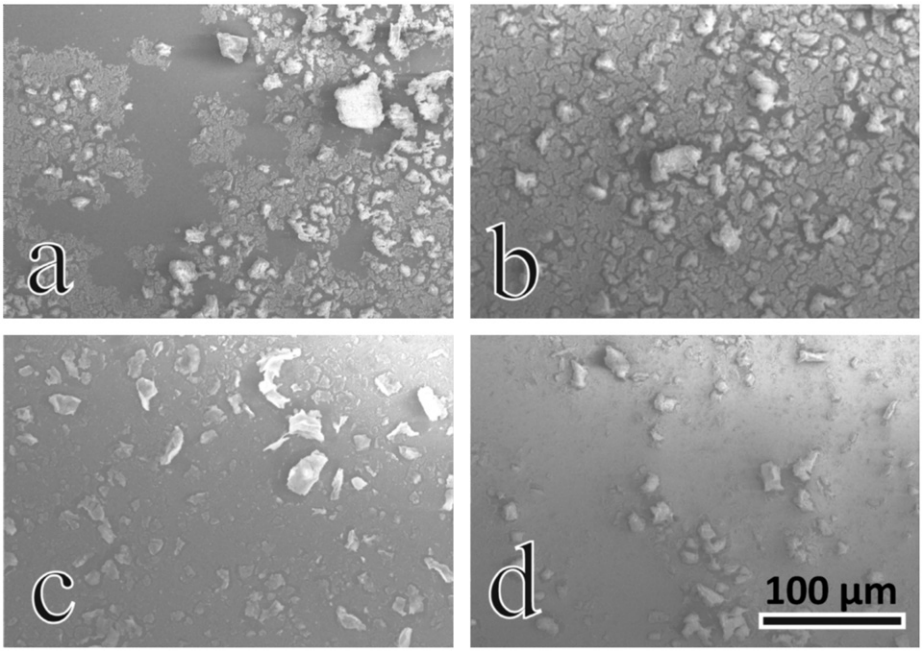

Fig. 5. Samples deposited by the spin-coating method on silicon substrates one week after the preparation of the sols. Samples prepared in isopropanol and (a) 0 vol% AcOH, (b) 0.5 vol% AcOH, (c) 1.1 vol% AcOH and (d) 9.1 vol% AcOH. Scale bar is 100 μm and applies to all images.

of this difficulty, our approach consists in the calculation of the first derivative of the transmittance with respect to the energy, knowing that this represents the ratio of change in transmittance through the film as function of the change in the incident energy. Based on this, the minimum of the rate of transmittance corresponds to the maximum of the rate of absorbance. Briefly, the arguments can be presented as follows. The optical absorption coefficient, α, of the films is evaluated using the relation [42,43]

$$\alpha = [1/t]\ln[T/(1-R)^2] \quad (3)$$

where T is the transmittance, R the reflectance and t the film thickness. For Fe_2O_3 with indirect band gap [44,45], the absorption follows a power law of the form:

$$(\alpha h\nu) = B\left(h\nu - E_g\right)^2 \quad (4)$$

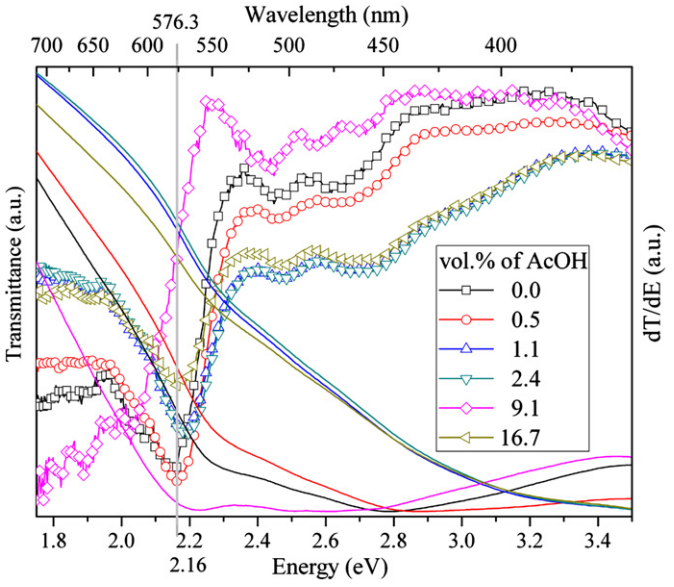

Fig. 6. UV–vis plots of samples deposited on glass on day 8. Continuous lines are transmittance and scatter and line correspond to the first derivative of transmittance over energy. Minimum of first derivative correspond to the maximum ratio of absorbance.

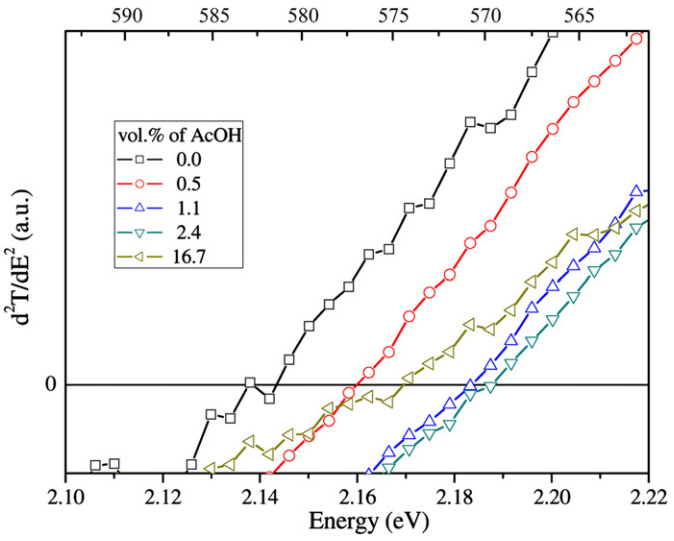

Fig. 7. Second derivative of transmittance over energy. The intersection of the plot indicates the maximum of absorption rate vs energy.

where hv is the energy of the incident photon, α the absorption coefficient, B the absorption edge width parameter, E_g the band gap. The second derivative of the optical absorption coefficient with respect to energy (i.e., $d^2\alpha/dE^2$) is positive. Specifically, the second derivative values of α using Eq. (4) are positive for $hv > E_g$. Following the concepts, we consider the value of the band gap to be the value of the maximum rate of absorbance. For this set of samples, the value of the band gap is ~2.16 eV, slightly below the reported value of the band gap for iron oxides (Fig. 6) [12,13]. The second derivative of the transmittance was calculated to know the exact value of the maximum absorbance and is presented in Fig. 7. In this plot, the exact value of the maximum of absorbance corresponds to the point where the trace crosses the abscissa. The difference between the smallest and the largest values of the band gaps is ~0.04 eV and a trend can be distinguished: the values increase in proportion of the concentration of AcOH from 0 to 2.4 vol% and decreases for higher values the value of the band gap.

4. Conclusions

Preparation, structural evaluation and optical analysis of α-Fe_2O_3 thin films in isopropyl alcohol with the addition of different concentrations of acetic acid is reported. XRD analysis confirms the presence of α-Fe_2O_3 as the unique phase composing the final material with an average grain size of 34 nm, independent of the concentration of AcOH. SEM images show the change of nanostructure of the materials related to the media of precipitation and the concentration of AcOH. The agglomeration of the nano-particles is dependent of the medium where precipitation occurs; water produce highly agglomerated particles meanwhile IsOH promotes the segregation of the particles and the nano-porosity of the material. The increase of the concentration of AcOH promotes the coarsening of the nano-particles and the reduction of porosity of the samples. UV–vis spectroscopy analysis indicates that the band gap of the materials is ~2.16 eV as expected for iron oxide (α-Fe_2O_3) phase. All the results confirm the procedure to be an efficient method of preparation of high quality and high porosity iron oxide films, without losing/modifying the grain size and the optical properties of the material.

References

[1] K. Sivula, R. Zboril, F. Le Formal, R. Robert, A. Weidenkaff, J. Tucek, J. Frydrych, M. Grätzel, Photoelectrochemical water splitting with mesoporous hematite prepared by a solution-based colloidal approach, Journal of the American Chemical Society 132 (2010) 7436–7444.

[2] A. Duret, M. Grätzel, Visible light-induced water oxidation on mesoscopic γ-Fe_2O_3 films made by ultrasonic spray pyrolysis, The Journal of Physical Chemistry B 109 (2005) 17184–17191.

[3] S.K. Mohapatra, S.E. John, S. Banerjee, M. Misra, Water photooxidation by smooth and ultrathin γ-Fe_2O_3 nanotube arrays, Chemistry of Materials 21 (2009) 3048–3055.

[4] Z. Wei, Z. Zhang, Q. Li, Y. Zhou, Y. Zhu, Enhanced photocatalytic activity of porous α-Fe_2O_3 films prepared by rapid thermal oxidation, Journal of Physics D: Applied Physics 41 (2008) 202002.

[5] R.L. Spray, K. Choi, Photoactivity of transparent nanocrystalline Fe_2O_3 electrodes prepared via anodic electrodeposition, Chemistry of Materials : A Publication of the American Chemical Society 21 (2009) 3701–3709.

[6] I. Cesar, A. Kay, J.A. Gonzalez Martinez, M. Grätzel, Translucent thin film Fe_2O_3 photoanodes for efficient water splitting by sunlight: nanostructure-directing effect of Si-doping, Journal of the American Chemical Society 128 (2006) 4582–4583.

[7] C. Leygraf, M. Hendewerk, G.A. Somorjai, Photodissociation of water by p-and n-type polycrystalline iron oxides by using visible light ($\leq$2.7 eV) in the absence of external potential, Proceedings of the National Academy of Sciences—Chemistry 79 (1982) 5739–5741.

[8] G. Wang, X. Gou, J. Horvat, J. Park, Facile synthesis and characterization of iron oxide semiconductor nanowires for gas sensing application, Journal of Physical Chemistry C 112 (2008) 15220–15225.
[9] H. Tang, M. Yan, H. Zhang, S. Li, X. Ma, M. Wang, D. Yang, A selective NH_3 gas sensor based on Fe_2O_3–ZnO nanocomposites at room temperature, Sensors and Actuators B 114 (2006) 910–915.
[10] S.A. Halawy, S.S. Al-Shihry, M.A. Mohamed, Gas-phase decomposition of formic acid over α-Fe_2O_3 catalysts, Catalysis Letters 48 (1997) 247–251.
[11] K.M. Parida, G.K. Pradhan, G.K. Sol–gel, synthesis and characterization of mesoporous iron–titanium mixed oxide for catalytic application, Materials Chemistry and Physics 123 (2010) 427–433.
[12] G.V. Samsonov, The Oxide Handbook, Plenum Data Company, New York, USA, 1982.
[13] M. Preisinger, M. Krispin, T. Rudolf, S. Horn, D.R. Strongin, Electronic structure of nanoscale iron oxide particles measured by scanning tunneling and photoelectron spectroscopies, Physical Review B 71 (2005) 165409–165415.
[14] G.K. Pradhan, K.M. Parida, Fabrication, growth mechanism, and characterization of α-Fe_2O_3 nanorods, ACS Applied Materials and Interfaces 3 (2011) 317–323.
[15] H.E. Prakasam, O.K. Varghese, M. Paulose, G.P. Mor, C.A. Grimes, Synthesis and photoelectrochemical properties of nanoporous iron (III) oxide by potentiostatic anodization, Nanotechnology 17 (2006) 4285–4291.
[16] Y. Maeda, Y. Morinaga, Y. Tomita, K. Kobayashi, Photoanodic response of iron oxide electrode in aqueous solution and its application to Pb^{2+} removal under visible light irradiation, Electrochimica Acta 54 (2009) 1757–1761.
[17] B.A. Balkoz, K.M. Clarkson, The effect of doping with Ti(IV) and Sn(IV) on oxygen reduction at hematite electrodes, Journal of the Electrochemical Society 148 (2001) E85–E91.
[18] A. Kleiman-Shwarsctein, Y. Hu, A.J. Forman, J.D. Stucky, E.W.J. McFarland, Electrodeposition of α-Fe_2O_3 doped with Mo or Cr as photoanodes for photocatalytic water splitting, Journal of Physical Chemistry C 112 (2008) 15900–15907.
[19] W.B. Ingler Jr., S.U.M. Khan, Photoresponse of spray pyrolytically synthesized copper-doped γ-Fe_2O_3 thin film electrodes inwater splitting, International Journal on Hydropower and Environment 30 (2005) 821–827.
[20] H.M. Fan, G.J. You, Y. Li, Z. Zheng, H.R. Tan, Z.X. Shen, S.H. Tang, Y. Feng, Shape-controlled synthesis of single-crystalline γ-Fe_2O_3 hollow nanocrystals and their tunable optical properties, Journal of Physical Chemistry C 113 (2009) 9928–9935.
[21] G.K. Mor, H.E. Prakasam, O.K. Varghese, K. Shankar, C.A. Grimes, Vertically oriented Ti–Fe–O nanotube array films: toward a useful material architecture for solar spectrum water photoelectrolysis, Nano Letters 7 (2007) 2356–2364.
[22] J. Yu, X. Yu, B. Huang, X. Zhang, Y. Dai, Hydrothermal synthesis and visible-light photocatalytic activity of novel cage-like ferric oxide hollow spheres, Crystal Growth and Design 9 (2009) 1474–1480.
[23] W. Du, Y. Xu, Y. Wang, Photoinduced degradation of orange II on different Iron (Hydr)oxides in aqueous suspension: Rate enhancement on addition of hydrogen peroxide, silver nitrate, and sodium fluoride, Langmuir 24 (2008) 175–181.
[24] M. Gotić, S. Musić, Synthesis of nanocrystalline iron oxide particles in the iron(III) acetate/alcohol/acetic acid system, European Journal of Inorganic Chemistry 6 (2008) 966–973.
[25] E. Thimsen, S. Biswas, C.S. Lo, P. Biswas, Predicting the band structure of mixed transition metal oxides: theory and experiment, Journal of Physical Chemistry C 113 (2009) 2014–2021.
[26] B.L. Cushing, V.L. Kolesnichenko, C.J. O'Connor, Recent advances in the liquid-phase syntheses of inorganic nanoparticles, Chemical Reviews 104 (2004) 3893–3946.
[27] J.P. Jolivet, S. Cassaignon, C. Chanéac, D. Chiche, E. Tronc, Design of oxide nanoparticles by aqueous chemistry, Journal of Sol–Gel Science and Technology 46 (2008) 299–305.
[28] J.P. Jolivet, C. Froidefond, A. Pottier, C. Chanéac, S. Cassaignon, E. Tronc, P. Euzen, Size tailoring of oxide nanoparticles by precipitation in aqueous medium. A semi-quantitative modeling, Journal of Materials Chemistry 14 (2004) 3281–3288.
[29] M. Niederberger, Nonaqueous sol–gel Routes to metal oxide nanoparticles, Accounts of Chemical Research 40 (2007) 793–800.
[30] N. Pinna, M. Niederberger, Surfactant-free nonaqueous synthesis of metal oxide nanostructures, Angewandte Chemie International 47 (2008) 5292–5304.
[31] G. Carbajal-Franco, C.V. Ramana, Synthesis and structural characterization of Fe–O nanonetworks, Journal of Vacuum Science and Technology A, Vacuum, SURfaces, and Films 28 (2010) 984–988.
[32] R.S. Shafik, M.S. Rahman, A.R. Islam, On the extended relationships among EVM, BER and SNR as performance metrics, in: Proceedings of the 4th International Conference on Electrical and Computer Engineering, 2006, pp 408–411.
[33] R. Marin, An efficient algorithm to estimate the instantaneous SNR of speech signals, in: Proceedings of the EUROSPEECH, 1993, 1093–1096.
[34] J. Ohtsubo, T. Asakura, Statistical properties of the sum of partially developed speckle patterns, Optics Letters 1 (3) (1993) 98–100.
[35] A.L. Patterson, The diffraction of X-rays by small crystalline particles, Physical Review 56 (1939) 972–977.
[36] A.L. Patterson, The Scherrer formula for X-ray particle size determination, Physical Review 56 (1939) 978–982.
[37] G.W. Simmons, B.C. Beard, Characterization of acid–base properties of the hydrated oxides on iron and titanium metal surfaces, Journal of Physical Chemistry 91 (1987) 1143–1148.
[38] M.T. Nguyen, D. Sengupta, G. Raspoet, L.G. Vanquickenborne, Theoretical study of the thermal decomposition of acetic acid: decarboxylation versus dehydration, Journal of Physical Chemistry 99 (1995) 11883–11888.
[39] N.I. Butkovskaya, G. Manke, D.W. Setser, Observation of the unimolecular decomposition pathways of chemically activated acetic acid by fourier transform infrared emission spectrometry, Journal of Physical Chemistry 99 (1995) 11115–11121.
[40] C.J. Brinker, Sol–Gel Science. The Physics and Chemistry of Sol–Gel processing, Academic Press, Inc., USA, 1990.
[41] J. Garcia-Solé, L.E. Bausá, D. Jaque, An Introduction to the Optical Spectroscopy of Inorganic Solids, John Wiley & Sons: Chicester, UK, 2005.
[42] S.K. Gullapalli, R.S. Vemuri, C.V. Ramana, Structural transformation induced changes in the optical properties of nanocrystalline tungsten oxide thin films, Applied Physics Letters 96 (2010) 171903–1–171903–3.
[43] P. Tyagi, A.G. Vedeshwar, Effect of residual stress on the optical properties of CdI_2 films, Physical Review B 66 (2002) 075422–1–075422-8.
[44] J.E. Turner, M. Hendewerk, J. Parmeter, D. Neiman, G.A. Somorjai, The characterization of doped iron oxide electrodes for the photodisscoiation of water, Journal of the Electrochemical Society 131 (1984) 1777–1783.
[45] A.A. Tahir, K.G. Upul Wijayantha, S. Saremi-Yarahmadi, M. Mazhar, V. McKee, Chemistry of Materials 21 (2009) 3763–3772.